This is a pre-copyedited, author-produced version of an article accepted for publication in Bulletin of Engineering Geology and the Environment following peer review. The final authenticated version is available online at https://doi.org/10.1007/s10064-021-02371-7.

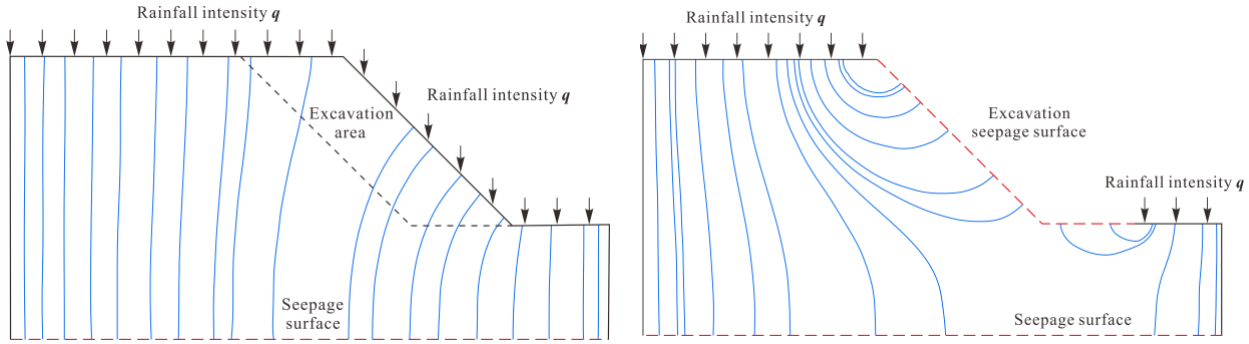

(a) Before excavation **(b) After excavation**

Fig. 1 Schematic diagram of seepage path changes in unsaturated soil slope excavation simulation

(Blue lines in the figure are the seepage lines)

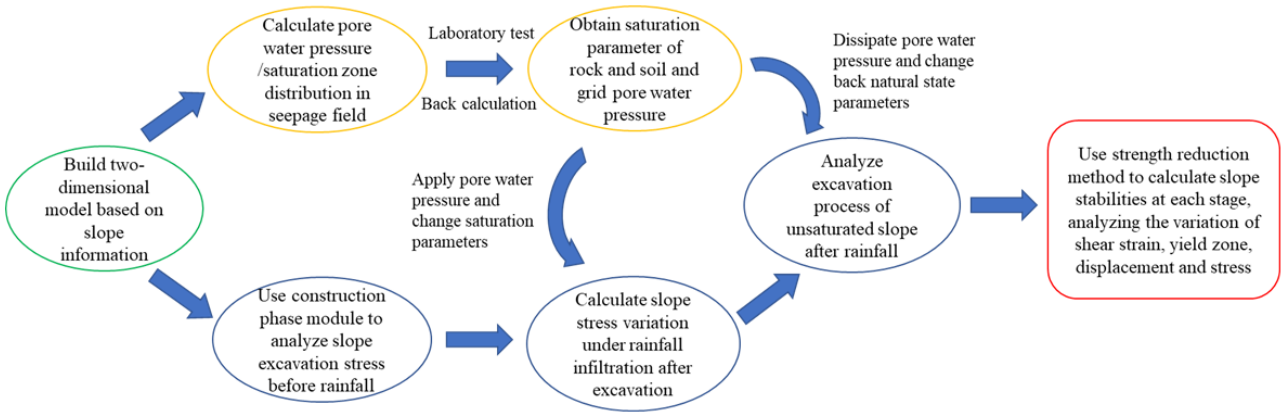

Fig. 2 Slope stability simulation process under alternating excavation and rainfall

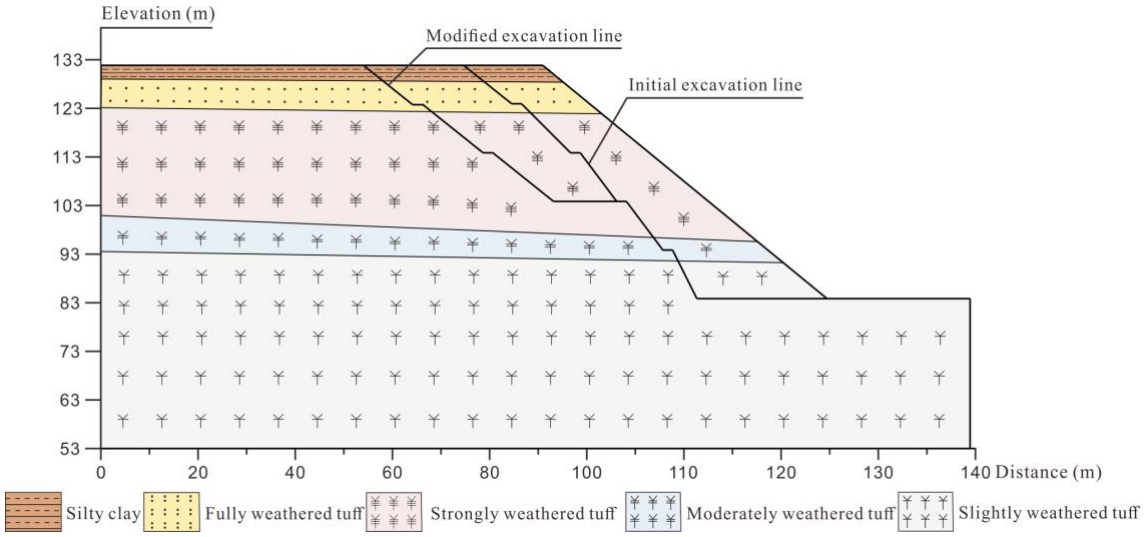

Fig. 3 Slope morphology and engineering geological conditions

(a) **(b)**

Fig. 4 Status of the slope sliding area in January 2015

(a) **(b)**

Fig. 5 Development of the slope sliding area from May to June 2015

(a) **(b)**

Fig. 6 Status of the slide after the modified excavation in January 2016

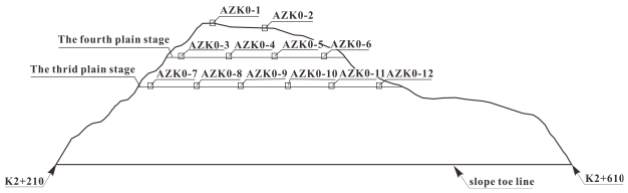

(a) Schematic diagram of the measuring point layout in the first and second stages

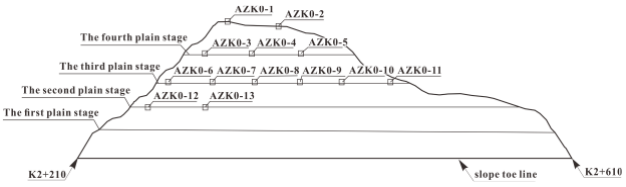

(b) Schematic diagram of the measuring point layout in the third stage

Fig. 7 Schematic diagrams of the measuring point layouts in each monitoring stage (AZK0-1 and 0-2 in the figure are newly added points in the second stage)

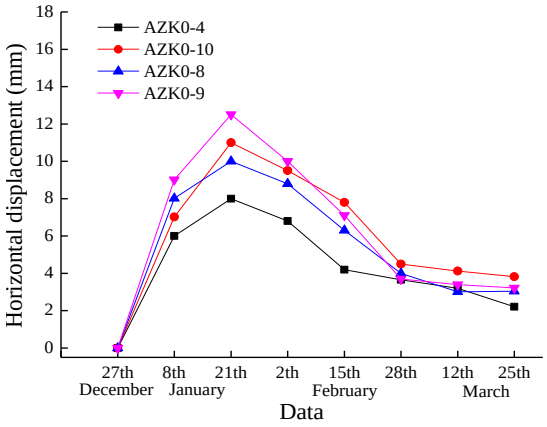

(a) The first monitoring stage

(December 2014 to March 2015)

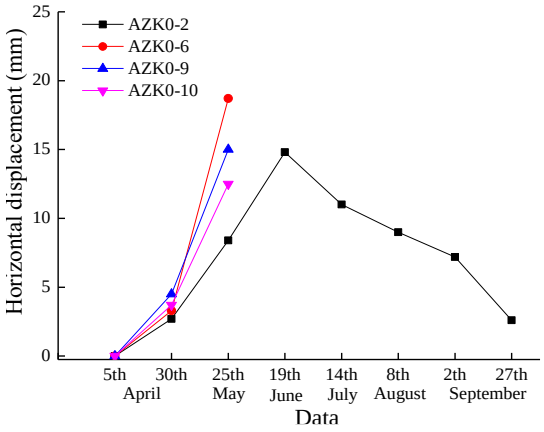

(b) The second monitoring stage

(April to September 2015)

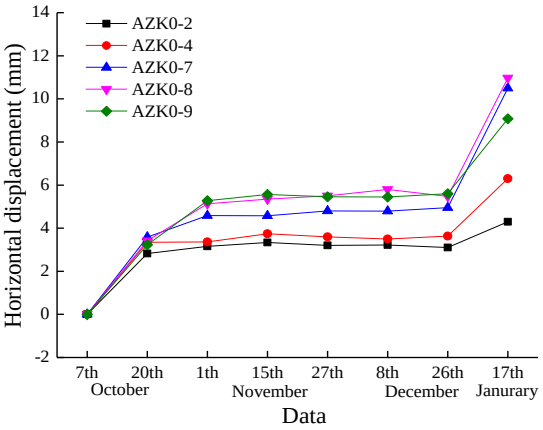

(c) The third monitoring stage

(October 2015 to January 2016)

Fig. 8 Horizontal displacements of typical measuring points during each stage

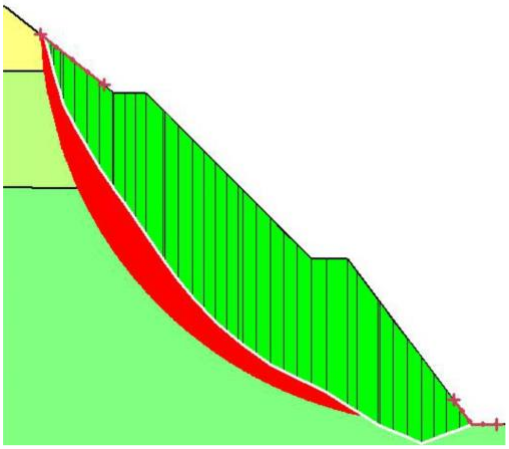

(a) The reduction ratio of 3:1

(F_s=0.998)

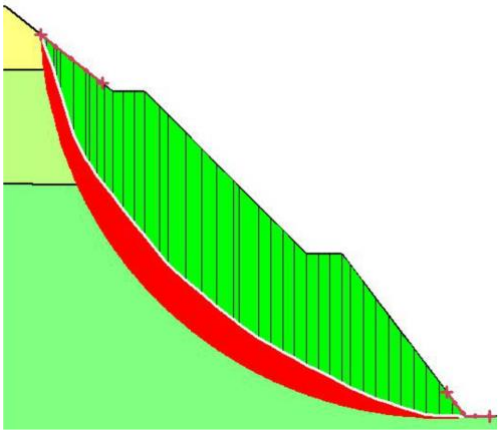

(b) The reduction ratio of 4:1

(F_s=0.982)

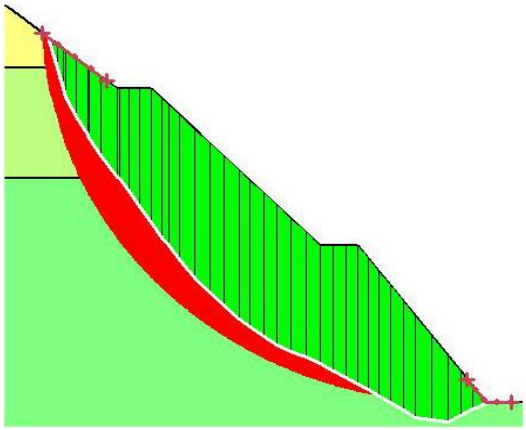

(c) The reduction ratio of 4:1

(F_s=0.994)

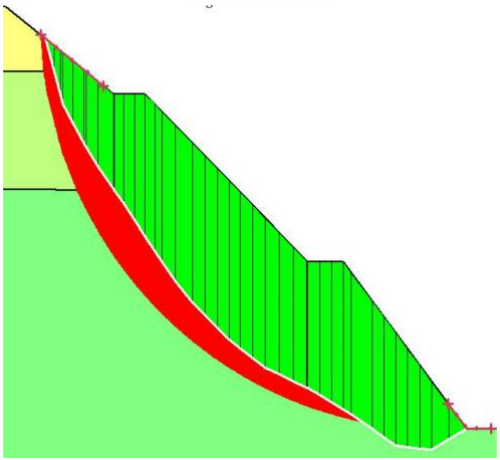

(d) The reduction ratio of 5:1

(F_s=0.996)

Fig. 9 Final sliding surfaces obtained by the inversion analysis

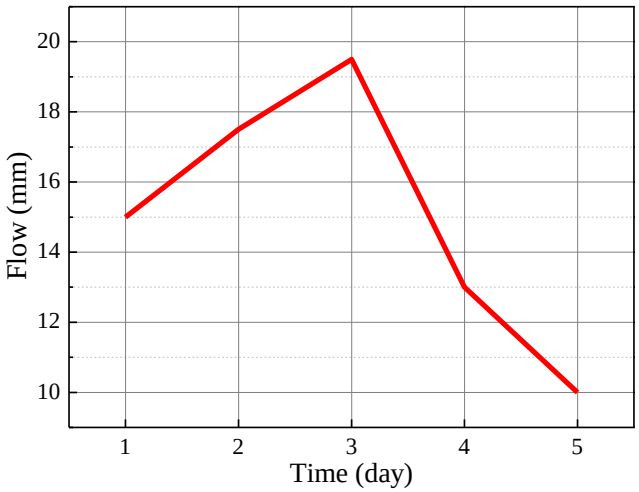

(a) First rainfall

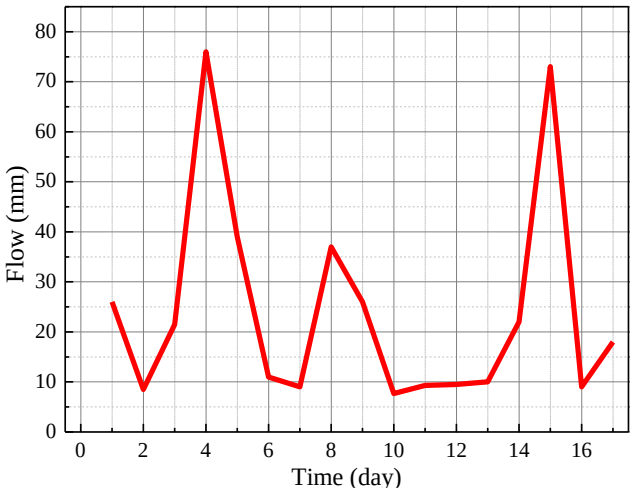

(b) Modified excavation rainfall

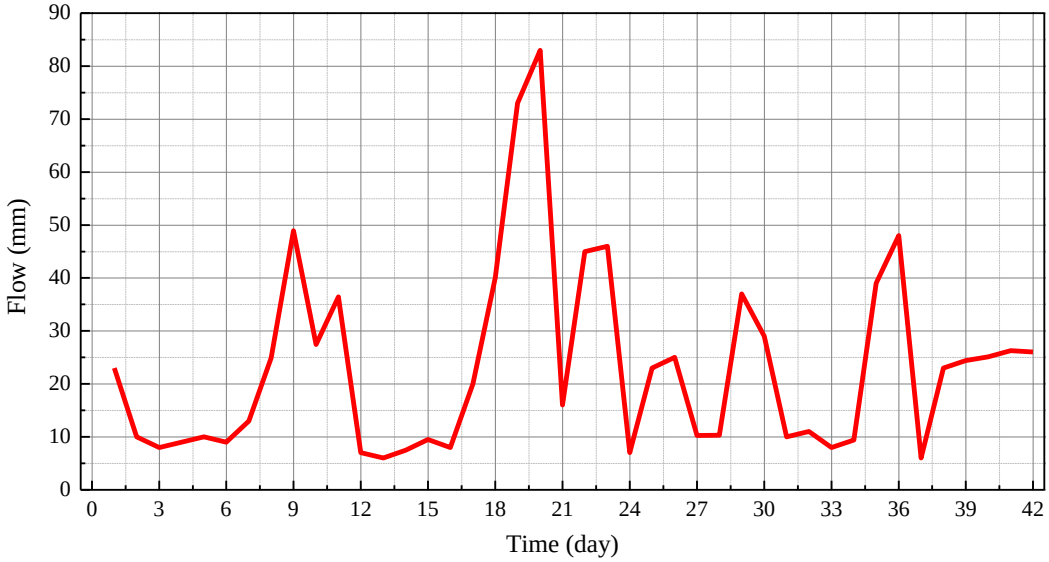

(c) Second rainfall

Fig. 10 The seepage boundary functions of the three rainfall events

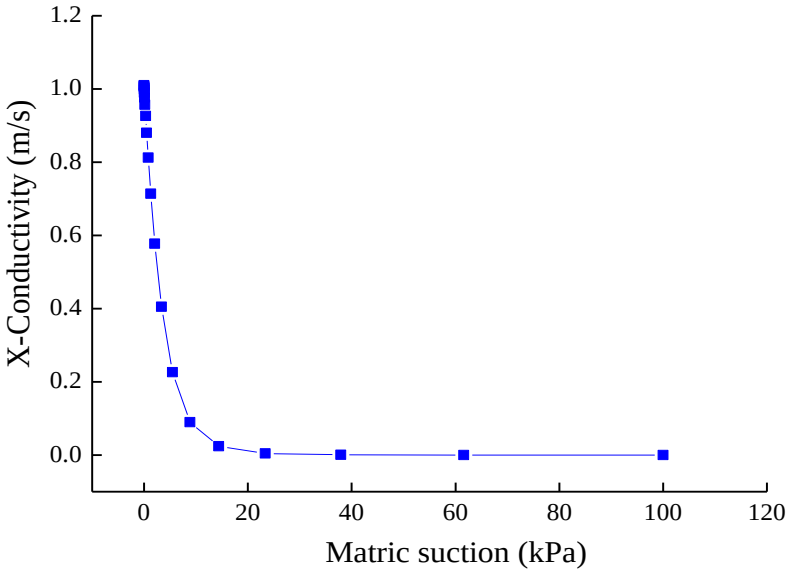

Fig. 11 Permeability function curve of the silty clay

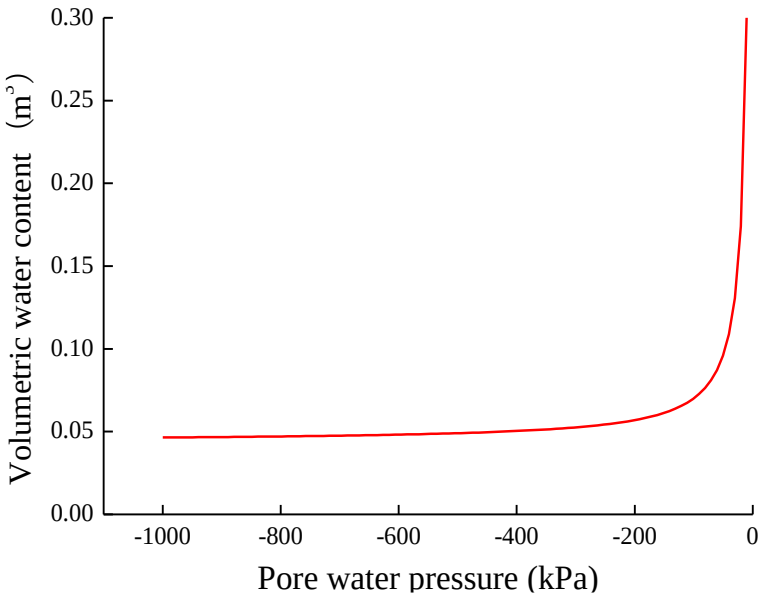

Fig. 12 Water content function curve of the silty clay

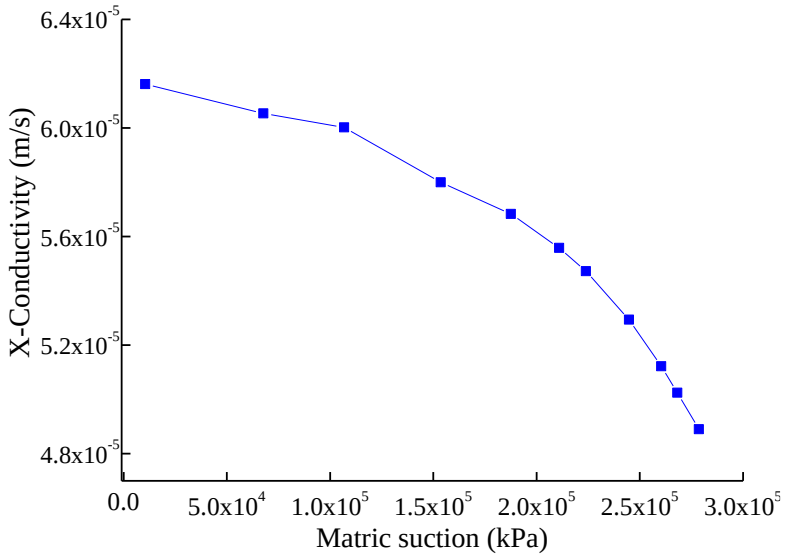

Fig. 13 Permeability function curve of the fully weathered tuff

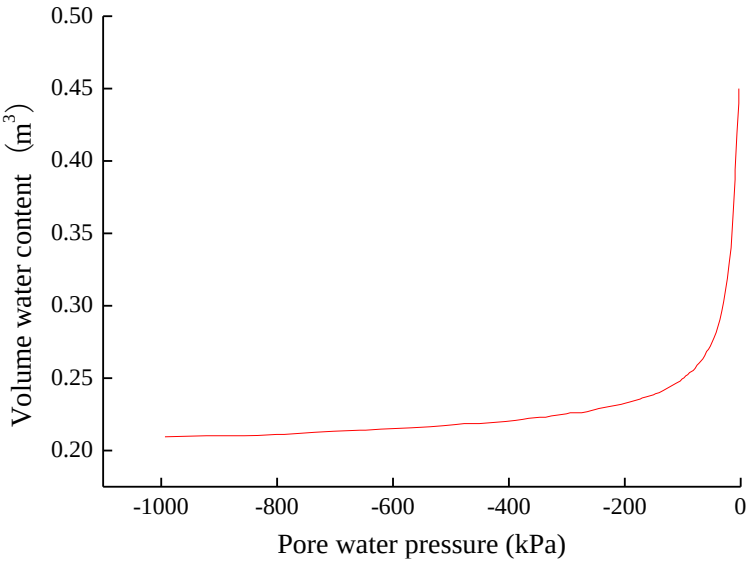

Fig. 14 Water content function curve of the fully weathered tuff

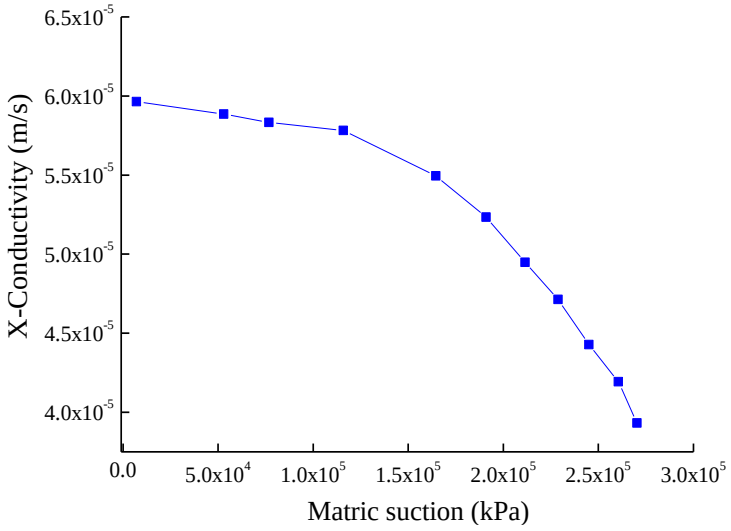

Fig. 15 Permeability function curve of the strongly weathered tuff

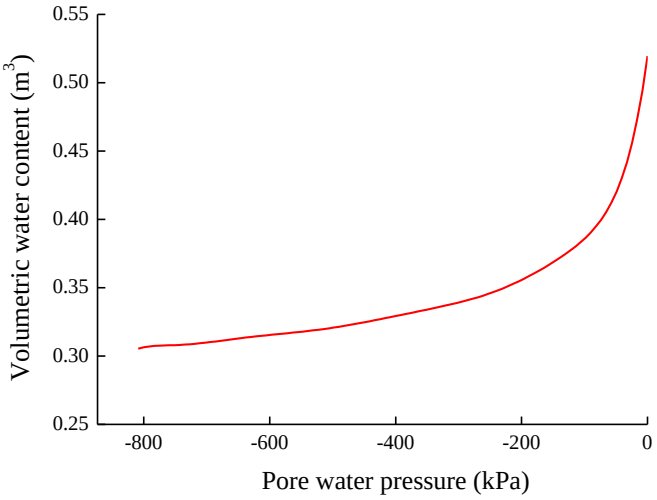

Fig. 16 Water content function curve of the strongly weathered tuff

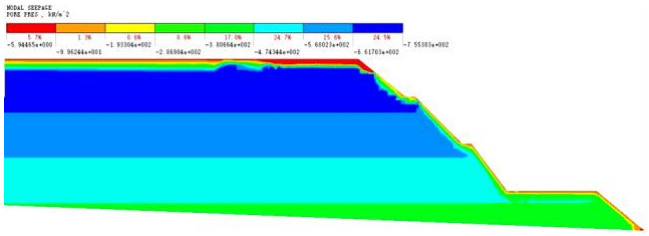

(a) First rainfall (day 1)

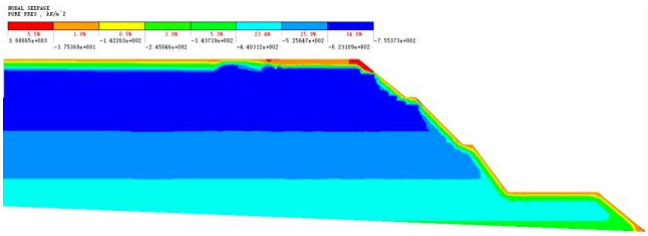

(b) First rainfall (day 3)

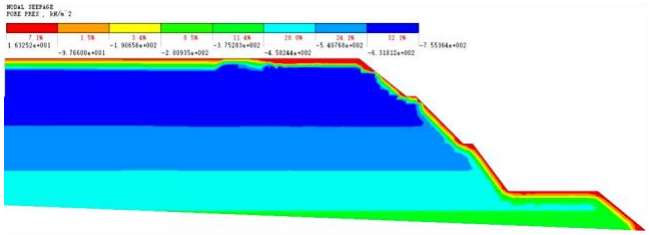

(c) First rainfall (day 5)

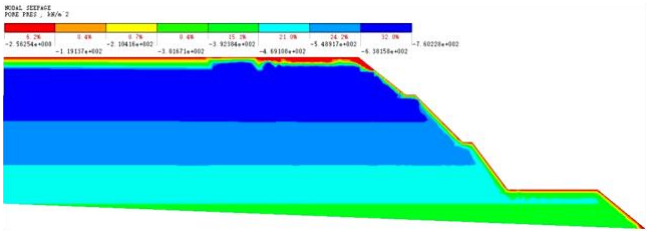

(d) Second rainfall (day 1)

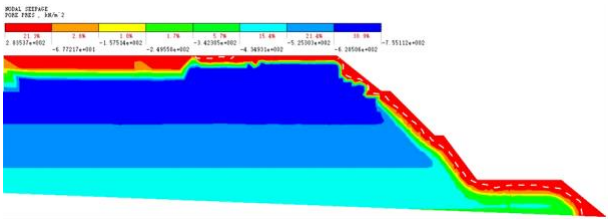

(e) Second rainfall (day 21)

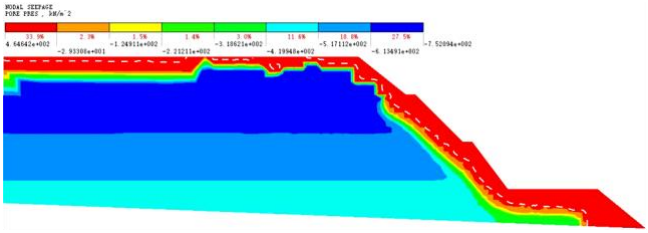

(f) Second rainfall (day 42)

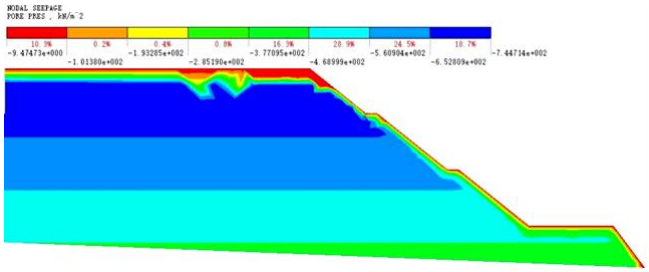

(g) Modified excavation rainfall (day 1)

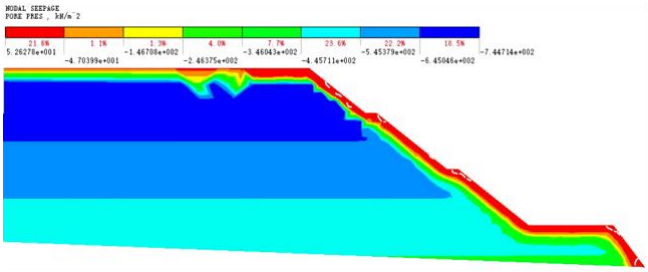

(h) Modified excavation rainfall (day 9)

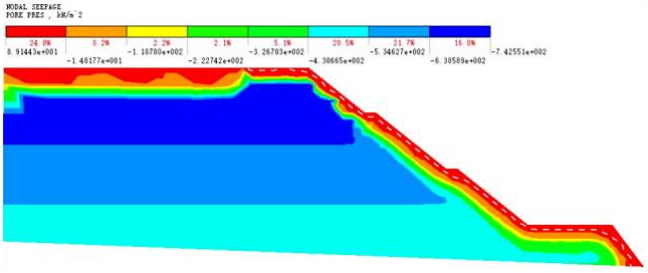

(i) Modified excavation rainfall (day 17)

Fig. 17 Pore water pressure distribution with time induced by three rainfall events

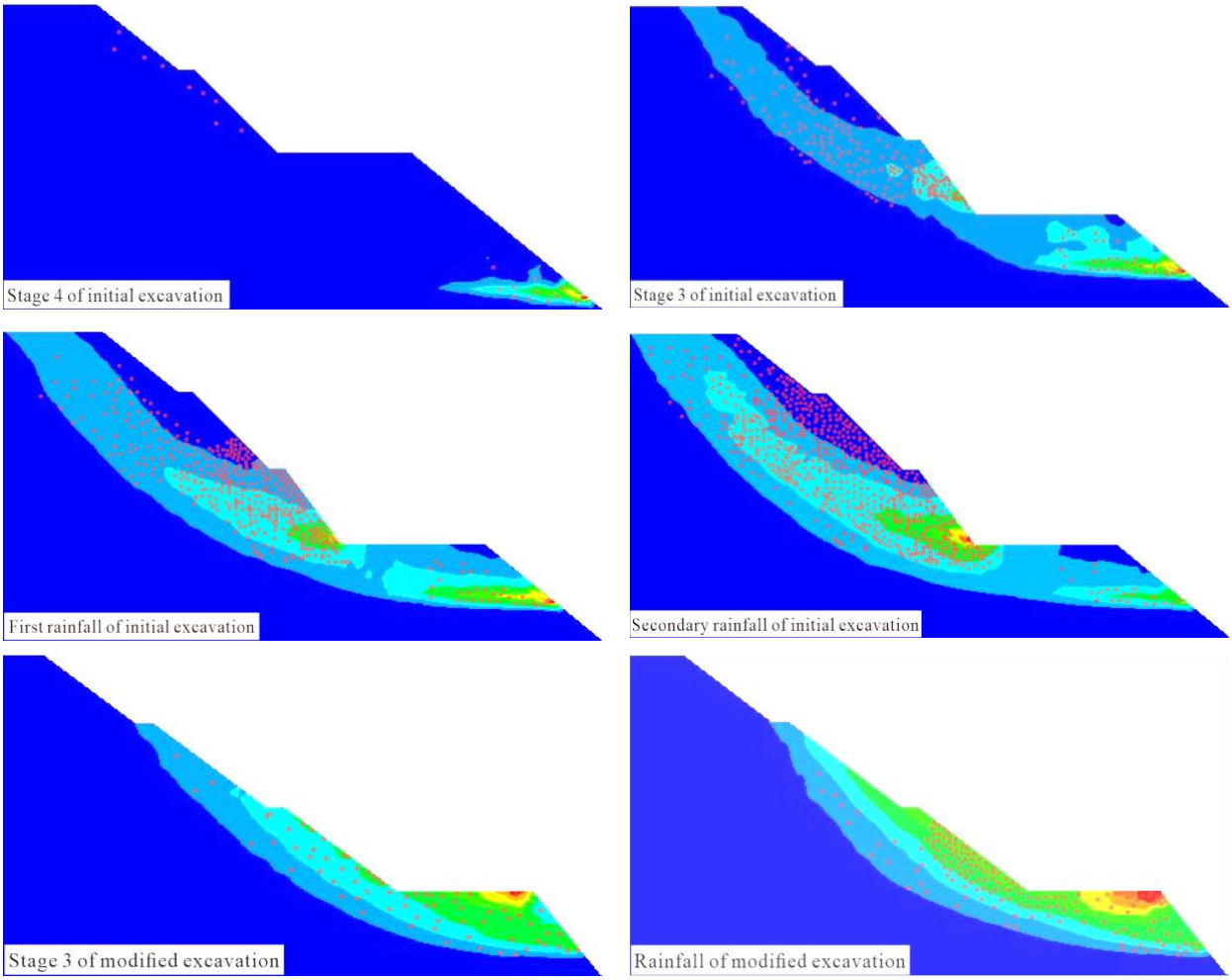

Fig. 18 Maximum shear strain and yield evolution in the slope (Red dots in the figures represent tensile yield elements)

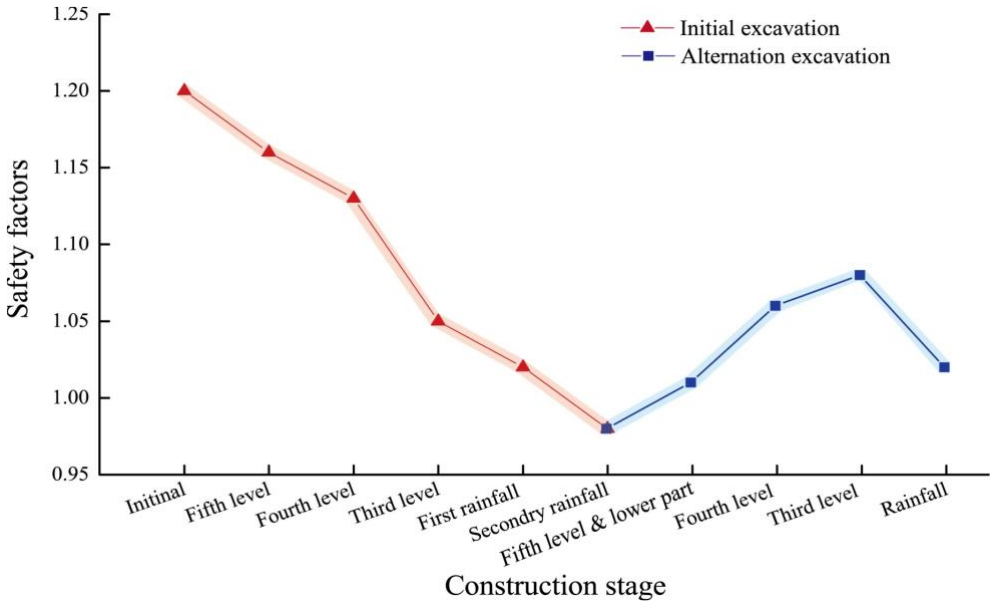

Fig. 19 Safety factor in each stage of the slope excavation sequence

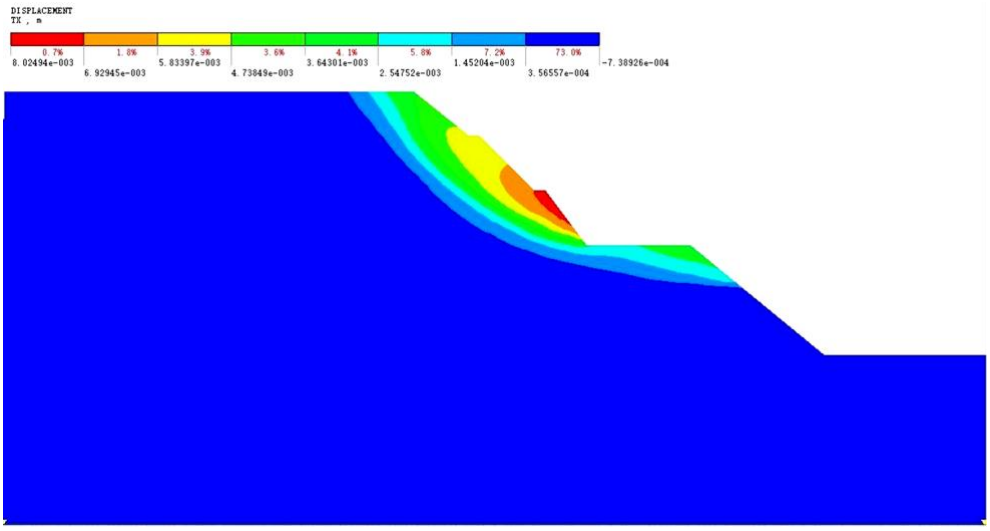

Fig. 20 Horizontal displacement distribution after initial excavation of the third-level slope

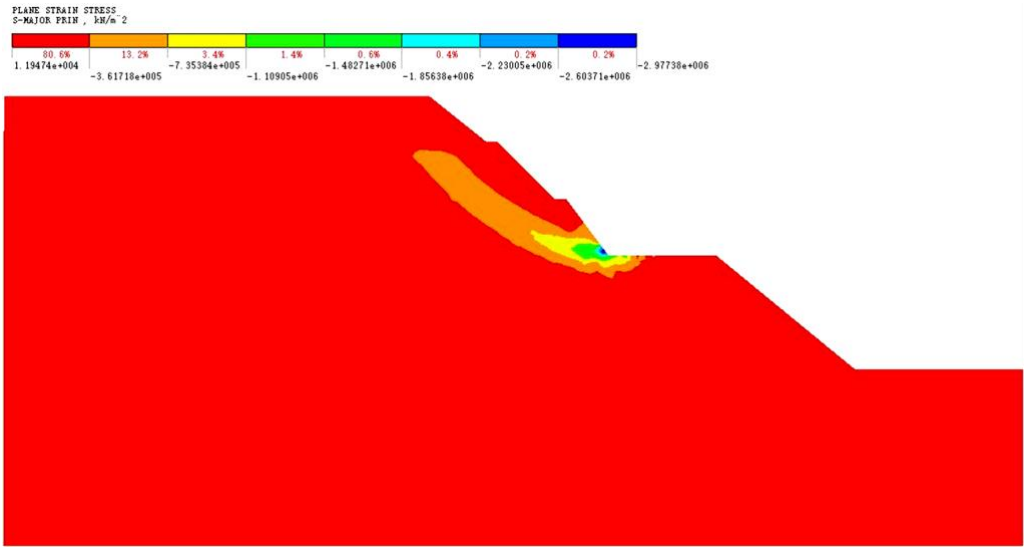

Fig. 21 Maximum principal stress distribution after initial excavation of the third-level slope

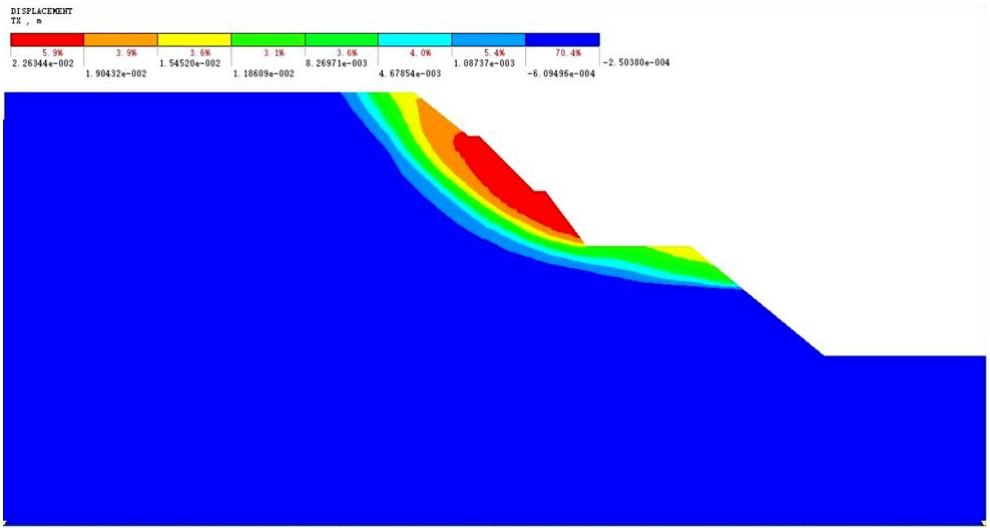

Fig. 22 Horizontal displacement distribution after the second rainfall

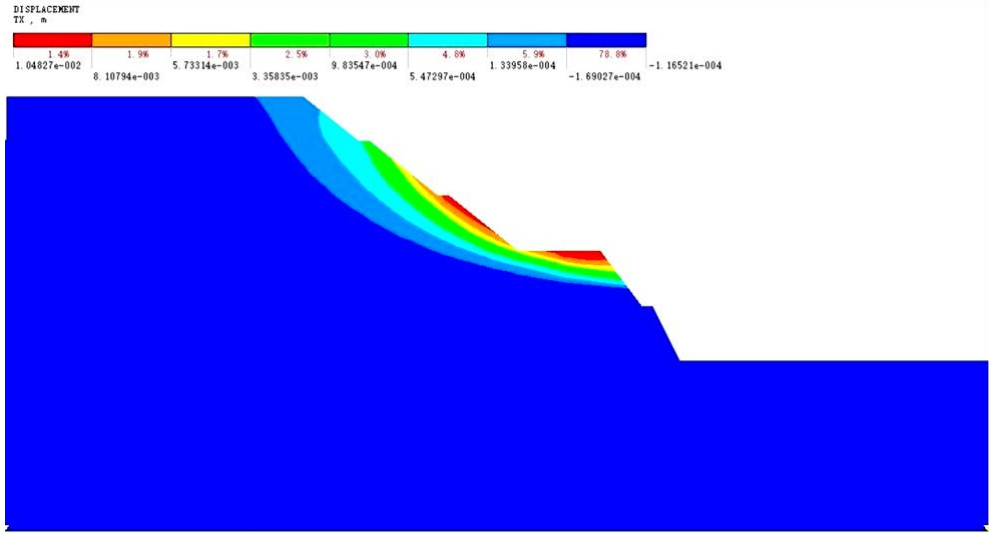

Fig. 23 Horizontal displacement distribution after the modified excavation rainfall